A Heton Model of the Spreading Phase of Open-Ocean Deep Convection

SONYA LEGG AND JOHN MARSHALL

Center for Meteorology and Physical Oceanography, and Department of Earth, Atmospheric and Planetary Sciences, Massachusetts Institute of Technology, Cambridge, Massachusetts

(Manuscript received 26 December 1991, in final form 1 July 1992)

ABSTRACT

A point-vortex *heton* model of the lateral dispersion of cold water formed in open-ocean deep convection is developed and studied as an idealized representation of the *sinking and spreading* phase of open-ocean deep convection. The overturning and geostrophic adjustment of dense fluid on and below the radius of deformation scale, formed by cooling on the large-scale, are parameterized in the model by introducing paired, discrete point vortices (hetons) of cyclonic sense in the surface layer, anticyclonic below, driving a cold baroclinic vortex. The convection site is imagined to be made up of many such baroclinic vortices, each with a vertically homogeneous core carrying cold, convectively tainted waters. The point vortices are introduced at a rate that depends on the large-scale cooling and the intensity assumed for each vortex. The interaction of many cold baroclinic vortices, making up a cloud, is studied using point-vortex Green's function techniques. The current solenoids of the individual elements sum together to drive a large-scale rim current around the convection site, cyclonic above, anticyclonic below, which is associated with a baroclinic zone on a scale of the order of the ambient radius of deformation. For parameters typical of open-ocean deep convection, the cloud of point vortices breaks down baroclinically on a time scale of a few days, into Rossby radius–scale "clumps." These extended hetons efficiently flux the cold water away laterally from the convection site and affect an inward transfer of heat sufficient to offset loss to the atmosphere.

1. Introduction

Observations of deep wintertime convection in the weakly stratified waters of the Gulf of Lions (Stommel et al. 1971; Schott and Leaman 1991) have revealed a rich structure on the smallest resolvable scales. In response to the dry, cold winds of the mistral, intense downwelling on scales of ~ 1 km have been observed, lasting only a few hours. They indicate that the response of the ocean to large-scale cooling is to sink in localized regions and are suggestive of the following scenario, schematized in Fig. 1.

Suppose that a weakly stratified ocean is subject to vigorous cooling at its surface, producing a density inversion and the possibility of overturning. Because of constraints due to the earth's rotation and the finite ocean depth (Chandrasekhar 1961), the fluid cannot overturn on the scale of the cooling (some hundreds of kilometers); rather the qualitative description must be that the response to widespread cooling is one in which relatively small-scale convection cells develop. The detailed physics that sets the convection scale is unclear at present. In linear rotating Rayleigh–Taylor theory (Davey and Whitehead 1981) the preferred scale depends on the chosen levels of eddy viscosity and thermal diffusivity and the depth assumed for the unstable layer. In laboratory (Fernando et al. 1991) and numerical simulations of rotationally controlled convection in a neutral ocean (see the accompanying paper by Jones and Marshall 1993) the scale $l_{\text{rot}} = (B_o/f^3)^{1/2}$, where B_o is the buoyancy forcing and f is the Coriolis parameter, emerges as an important scale. Modulation of the near-surface stratification on the scale of the ambient Rossby radius of deformation, typically a few kilometers, may also be important in preconditioning the flow on geostrophic scales and imposing a scale.

Whatever the precise details that set the scale of deep-reaching convective plumes, observations suggest that it is a significant fraction of the local radius of deformation, since deep convective overturning occurs in a fluid that is already very weakly stratified. For example, the Brunt–Väisälä frequency of the ambient waters in the Gulf of Lions can fall below $N \sim 10^{-4}\ \text{s}^{-1}$ (see Schott and Leaman 1991), corresponding to a Rossby radius $L_\rho = NH/\pi f$ of ≤ 1 km if the local depth is 2 km. This is the scale on and above which rotation must be important (see Table 1 of Jones and Marshall 1993, hereafter JM). Thus, the convectively tainted water will, on a time scale of $\sim f^{-1}$, come increasingly under geostrophic control, forming a baroclinic vortex that

Corresponding author address: Sonya Legg, Joint Institute for Laboratory Astrophysics, University of Colorado, Boulder, CO 80309.

© 1993 American Meteorological Society

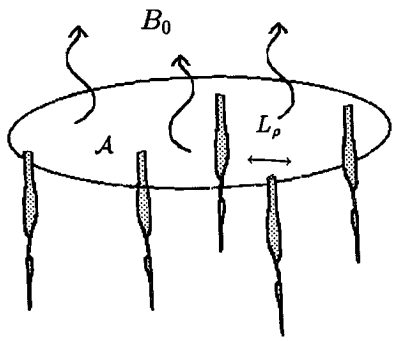

FIG. 1. A schematic diagram of the convection site of area A exposed to buoyancy loss at a rate B_o, peppered by a population of plumes sinking on scales that are a significant fraction of the local radius of deformation L_ρ.

is susceptible to baroclinic instability (Killworth 1976; Gascard 1978).

Figure 2 shows a sequence of temperature sections charting, over a three-day period, the development and geostrophic adjustment of a baroclinic vortex triggered by surface buoyancy loss in a weakly stratified ocean with an $L_\rho = 1.4$ km. It has been obtained numerically using a nonhydrostatic primitive equation model designed specifically for the study of plume-scale convection in the presence of rotation [see Brugge et al. (1991) and JM for a full discussion of the model used]. Details of model parameters, stratification, and forcing functions can be found in the legend of Fig. 2. Fluid exposed to cooling becomes constrained by the earth's rotation and trapped in a vorticular motion. Cooled at the surface, fluid eventually becomes sufficiently dense to sink toward its neutrally buoyant level. The vertically homogeneous column of fluid generated in the initial overturning phase subsequently adjusts under the influence of gravity and rotation; vertical exchange of fluid in the column is replaced by azimuthal currents circulating around the cold mixed core in balance with its radial pressure gradient (see Fig. 3, which shows the end state in gradient wind balance after convection has ceased). The sides of the column, which after the initial rapid overturning were vertical, have, after three days, slumped as dense fluid tries to sink down but is inhibited by the earth's rotation. They slope, over the depth of the column, by a distance comparable to L_ρ, as one would expect from geostrophic adjustment theory (Dewar and Killworth 1991).

We see, then, that the initial convective activity on the plume scale, in which fluid is exchanged vertically, is succeeded on time scales $\geq f^{-1}$ by a balanced vorticular motion; only a "fossil record" of previous vertical mixing remains in the homogeneous core of the geostrophically adjusted plume. In this contribution we study the fate of a population of such adjusted vortices, as represented schematically in Fig. 1, in an idealized model of the *sinking and spreading* phase of open-ocean deep convection. Viewed from the large scale each geostrophically adjusted plume must appear as a delta function of coldness and vorticity. The radius of influence of each chimney will be controlled by the local deformation radius—a few kilometers. If the average separation between the plumes is of the order of L_ρ, then they will "feel" the presence of one another and begin to interact. The interaction of a cluster of mature plumes is studied by developing a two-layer point-vortex *heton* model (Hogg and Stommel 1985a,b) using Green's functions. In this model the potential vorticity structure of the adjusted vortex is represented by a positive vorticity anomaly in the upper layer and a negative anomaly in the lower layer.

In section 2 we examine in detail the potential vorticity structure of a convectively created baroclinic vortex and demonstrate, by inverting prescribed potential vorticity distributions to obtain the flow and density fields, that it may be represented by a highly idealized PV distribution, with a positive anomaly in potential vorticity at the surface, negative below. In section 3 the heton model is described; hetons are randomly introduced over a specified convection patch at a rate that depends on the large-scale heat loss and the intensity of the individual elements. Experiments enquiring into the interaction of individual elements of a population of such hetons and their ultimate breakup by baroclinic instability are described in section 4. We find that populations of balanced plumes cluster together in Rossby radius scale clumps and organize themselves to efficiently flux heat and stratified fluid from the surroundings into the convection site, offsetting the heat loss from the surface and bringing in convectively unmodified water to be processed in the chimney.

2. A potential vorticity perspective

In order to develop a simplified model of a geostrophically adjusted vortex, we first examine its potential vorticity structure. There are some subtleties here that must be handled with care. Consider that fluid making up the vortex that is enclosed laterally by an angular momentum surface and above and below by the sea surface and the ocean floor, as shown schematically in Fig. 4a. Angular momentum surfaces (defined by $M = fr^2/2 + rv$, where f is the Coriolis parameter and v is the azimuthal velocity at radius r) are chosen to define our volume because, in inviscid axisymmetric flow, they are material surfaces even in the presence of nonhydrostatic effects and diabatic heating (e.g., see Dewar 1987). The volume of fluid contained within an M surface is a constant in the inviscid limit. For example, Fig. 3b plots M surfaces before and after convective overturning in the numerical experiment described in the Introduction. The cylindrical M sur-

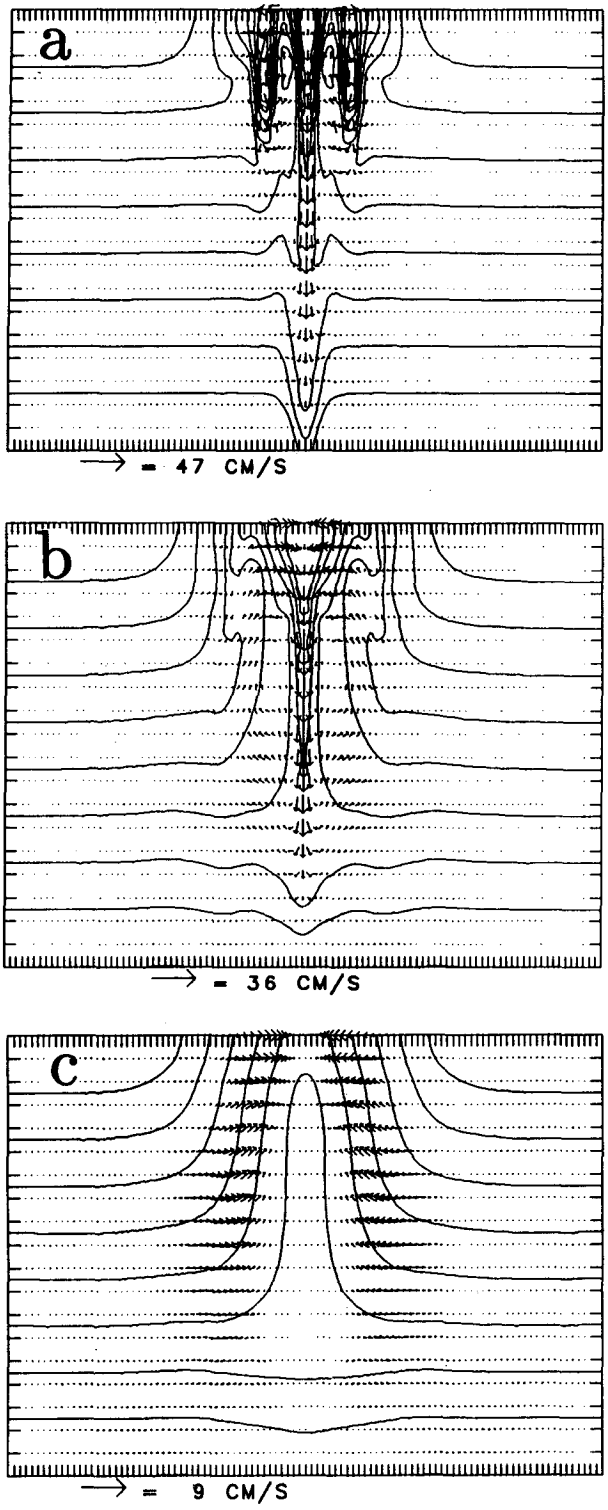

FIG. 2. Vertical sections charting the development of a baroclinic vortex in a numerical simulation at (a) day 1, (b) day 2, and (c) day 3. Temperature contours are plotted with vectors superimposed showing the velocity (u, w) in the plane of the section. The tick marks along the horizontal axis are every 250 m, those on the vertical axis every 100 m, at the resolution of the numerical model. The domain of integration is a doubly period box of 16 km square and 2 km in depth. The top to bottom temperature difference of the ambient fluid is 0.05 K implying an $N^2 = 5 \times 10^{-8}$ s^{-2} and a radius of deformation $L_\rho = NH/\pi f = 1.4$ km. An axisymmetric Gaussian pattern of cooling is applied for a period of two days at the ocean's surface, with a peak cooling rate of 800 Wm^{-2} decaying away with an e-folding scale of 2 km. Precise details of the model and the experiment presented here can be found in Brugge et al. (1991).

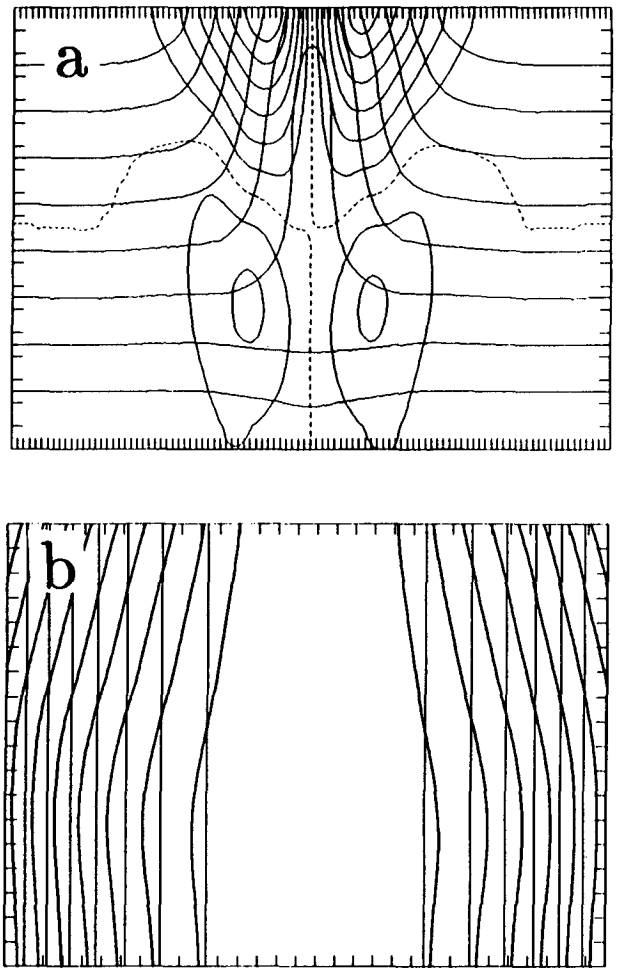

FIG. 3. The geostrophically adjusted end state, after convection has ceased, revealing the structure of the baroclinic vortex. In (a) temperature contours are plotted (in units of 0.05 K) with isopleths of velocity v normal to the section (in units of 1 cm s^{-1}) superimposed. We see a vertically homogeneous core with strong and cyclonic circulation in the upper half of the column, weak anticyclonic circulation below (the zero azimuthal velocity contour is dotted). In (b) angular momentum surfaces $M = fr^2/2 + rv$ in the initial resting fluid (concentric cylinders) at time $t = 0$ and at day 3 are plotted. Note that the horizontal scale in (b) has been expanded relative to (a).

faces of the initial resting fluid become pinched together in the near-surface layers as fluid, undergoing cooling, converges to sink to depth. Here there is a concentration of cyclonic vorticity. Beneath, at the base of the column, the M tubes have dilated as fluid diverges and

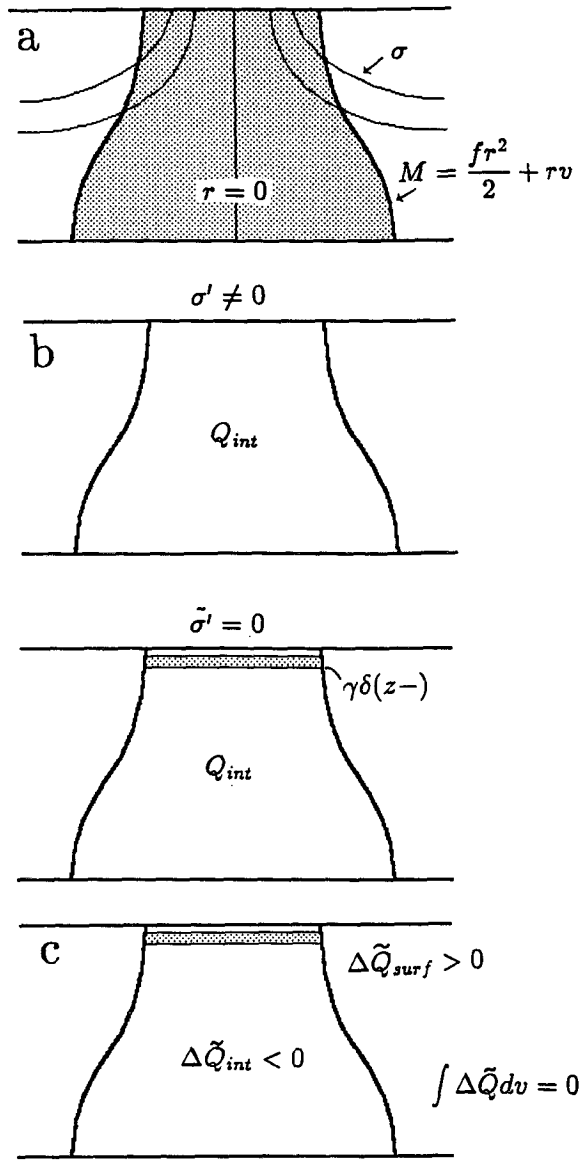

FIG. 4. Isopycnals σ and angular momentum surfaces M of a schematized axisymmetric baroclinic vortex are shown in (a). We consider the budget of potential vorticity within the shaded volume enclosed by angular momentum surfaces. The density anomaly at the surface σ' in (b) (i) is replaced by a delta-function sheet of potential vorticity just beneath an isothermal surface in (b) (ii). The effect of convective overturning of the column is to affect, as shown in (c), a redistribution of modified potential vorticity $\Delta\tilde{Q}$; it is evacuated from the interior of the fluid into a delta-function sheet of potential vorticity just beneath the isopycnal upper surface.

begins to spin more anticyclonically. To the extent that the numerical model is inviscid, the volume of fluid within each M surface is conserved; in the experiment described here the volume of fluid contained within a given M surface only changes by about 5% over the period of integration showing that viscous processes are not a controlling influence.

a. The budget of PV within a material volume

We now examine the change in the potential vorticity of the fluid within our control volume brought about by surface cooling. It is convenient to consider the flux form of the potential vorticity equation (Haynes and McIntyre 1987), which can be written, using the notation of Marshall and Nurser (1992),

$$\frac{\partial \rho Q}{\partial t} + \nabla \cdot \mathbf{J} = 0, \tag{1}$$

where $\mathbf{J} = \rho Q\mathbf{u} - g^{-1}B\omega + \mathbf{F} \times \nabla\sigma$ is a generalized potential vorticity flux including both advective and nonadvective contributions, $Q = -(1/\rho)\omega \cdot \nabla\sigma$ is the potential vorticity, $B = -gD\sigma/Dt$ is the buoyancy forcing, $\mathbf{F} = (D\mathbf{u}/Dt + 2\Omega \times \mathbf{u} + \rho^{-1}\nabla p)$ represents the applied body forces, $\omega = 2\Omega + \nabla \times \mathbf{u}$ is the absolute vorticity with Ω the rotation rate and $\mathbf{u}$ the velocity, and σ is the potential density. Setting $\mathbf{F}$ to zero,[1] we integrate (1) over a volume bounded laterally by an angular momentum surface, and above and below by the ocean surface and the ocean floor where we assume $B = 0$ (as represented schematically in Fig. 4a) to obtain

$$\frac{\partial}{\partial t}\int \rho Q dV = -\oint_{\text{sides}} \rho Q\mathbf{u} \cdot d\mathbf{A} + \int_{\text{top}} g^{-1}B\omega \cdot d\mathbf{A}. \tag{2}$$

The first term on the right-hand side of (2) is the potential vorticity flux out of the volume, which is identically zero, since we have chosen to integrate over a volume bounded by angular momentum surfaces, which are *material* surfaces. We therefore have a simple relation between the net rate of change of potential vorticity in our volume and the buoyancy forcing applied at the upper surface

$$\frac{\partial}{\partial t}\int \rho Q dV = \int_{\text{top}} g^{-1}B\omega \cdot d\mathbf{A}. \tag{3}$$

Thus, it can be seen that buoyancy loss at the surface ($B < 0$) will result in an overall *decrease* in the potential vorticity of the control volume.

It is highly informative to represent (following Bretherton 1966) the cold surface of the baroclinic vortex by an appropriate sheet of potential vorticity just beneath the sea surface, which can then be assumed to be an isopycnal surface. The adoption of such an isopycnal upper boundary condition leads to a great computational simplification because our problem is reduced to one of advecting around distributions of potential vorticity *interior* to the fluid. This device is, in fact, implicit in layered quasigeostrophic models, which are the basis of the idealized model presented in the next section. Accordingly we introduce a modified PV distribution denoted by $\tilde{Q}$, defined by

[1] We neglect both stresses applied at the ocean's surface and frictional forces at the ocean floor.

$$\tilde{Q} = Q_{\text{int}} + \gamma\delta(z-), \tag{4}$$

where Q_{int} is the PV distribution in the interior of the vortex, and $\gamma\delta(z-)$, a sheet of PV just beneath the sea surface, will represent the effect of surface density anomalies; $\tilde{Q}$ is to be inverted for the flow and density field using the following upper boundary condition:

$$\tilde{\sigma}'(x, y) \equiv 0 \tag{5}$$

at the surface where $\tilde{\sigma}'(x, y)$ is the modified perturbation density. The strength γ of the potential vorticity sheet can be determined by noting that if $\tilde{\sigma}' = 0$ the (modified) buoyancy forcing $\tilde{B}$ at the surface must also be zero, and hence from (3)

$$\frac{\partial}{\partial t}\int \rho\tilde{Q}dV = 0 \tag{6}$$

or

$$\int \rho\tilde{Q}dV = \text{const.} \tag{7}$$

Thus the quantity of $\tilde{Q}$ within our control volume is constant. The strength γ of the vortex sheet in (4) is therefore chosen to be just sufficient to satisfy (7). The equivalence of the two PV distributions is indicated schematically in Fig. 4b.

The use of $\tilde{Q}$ leads to a great conceptual, as well as computational, simplification because *the effect of the convective overturning of the column is simply to redistribute the $\tilde{Q}$ of the initially resting stratified fluid*—the $\tilde{Q}$ of the interior is evacuated onto the delta-function sheet just below the surface of the fluid. Surface temperature anomalies and interior PV anomalies can be treated simultaneously and in the same manner.

If the PV associated with the initial resting fluid $Q_0(z) = -(f/\rho_s)(d\sigma_0/dz)$ is separated out (here ρ_s is a constant reference density and σ_0 the ambient stratification), and the departure from it is denoted by $\Delta\tilde{Q}$, (7) implies that (replacing ρ by its reference value)

$$\int \Delta\tilde{Q}dV = 0. \tag{8}$$

Equations (3), (4), and (8) provide, through appropriate distributions of PV, a means of parameterizing the balanced circulation induced by convective overturning of the column after geostrophic adjustment has taken place. The form of the potential vorticity anomaly $\Delta\tilde{Q}$ is represented schematically in Fig. 4c. The negative anomaly in the interior of the fluid is a consequence of the reduction in the stratification there, due to the convective overturning of the column; the positive anomaly evacuated from the homogeneous core represents the cold surface.

The following example serves to illustrate the equivalence between a surface density distribution and a potential vorticity sheet beneath an isopycnic surface. We show in Fig. 5 the velocity and density fields resulting from two potential vorticity inversions, both of which model the structure of a geostrophically adjusted column. In each case a prescribed potential vorticity distribution was inverted subject to geostrophic and hydrostatic balance conditions, consistent with imposed lateral boundary conditions. Details of the inversion method and parameters are shown in the Appendix.

In Fig. 5a the potential density at the sea surface is specified and an idealized interior PV anomaly inverted to give the hydrography and azimuthal velocity of a baroclinic vortex. The assumed PV distribution and surface density field were chosen to be broadly consistent with the baroclinic vortex generated in our nonhydrostatic convection model (see the Appendix). The inverted hydrography and velocity structure broadly resembles that of the numerically generated vortex (cf. Fig. 3). In Fig. 5b, an interior PV field identical to that of Fig. 5a is used, but now the cold surface is represented by a sheet of high PV just beneath the upper boundary, which is prescribed to be an isopycnal surface. The strength of the high PV anomaly is chosen so that constraint (8) is satisfied. The inverted density and velocity fields (Fig. 5b) are almost identical to that of Fig. 5a, a small discrepancy arising due to the finite resolution at which the inversion is carried out. Note, however, that in Fig. 5b, unlike 5a, the isopycnals cannot cut the upper surface which is itself an isopycnal.

We now exploit this equivalence to idealize the potential vorticity anomaly field of the overturned column, employing a heton model in which the schematised PV anomaly field, Fig. 4c, is used in a two-layer model under quasigeostrophic dynamics.

b. *Quasigeostrophic scaling*

If $\text{Ro} \ll 1$ and $(\text{Ri Ro})^{-1} \ll 1$, where $\text{Ri} = N^2H^2/V^2$ and $\text{Ro} = V/f_0L$ are the Richardson and Rossby numbers, based on typical velocity V and horizontal and vertical scales L and H, respectively, then potential vorticity can be well approximated by [a useful outline of the arguments can be found in Berrisford et al. (1993)]

$$\rho Q = -\omega\cdot\nabla\sigma \approx -\frac{d\sigma_0}{dz}(f+q), \tag{9}$$

where

$$q = \nabla^2\psi + f_0{}^2\frac{\partial}{\partial z}\left(\frac{1}{N^2}\frac{\partial\psi}{\partial z}\right)$$
$$= \nabla^2\psi - \frac{gf_0}{\rho_s}\frac{\partial}{\partial z}\left(\frac{\sigma'}{N^2}\right) \tag{10}$$

is the quasigeostrophic potential vorticity, the perturbation about the constant planetary vorticity f, ψ is the

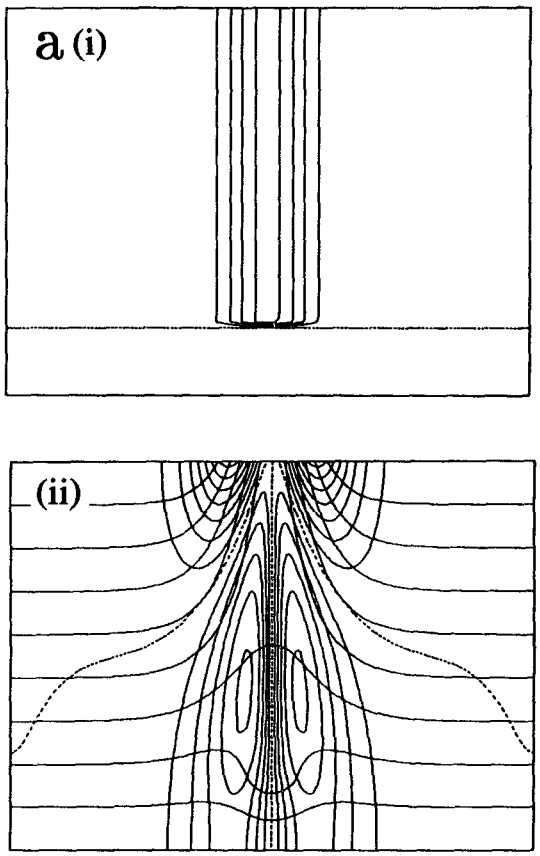

FIG. 5a. The idealized interior potential vorticity distribution shown in (i) is inverted to give the velocity and temperature fields of a baroclinic vortex shown in (ii); temperature is prescribed at the upper and lower boundaries and the azimuthal velocity is set to zero on vertical boundaries. At the core of the vortex we see isopycnals rising up to the surface; strong cyclonic flow reaching 7 cm s^{-1} is found at upper levels with somewhat weaker anticyclonic circulation below. The dotted contour is the zero contour with cyclonic circulation above it, anticyclonic below. The contour interval for velocity is 1 cm s^{-1}, and for temperature 0.005 K.

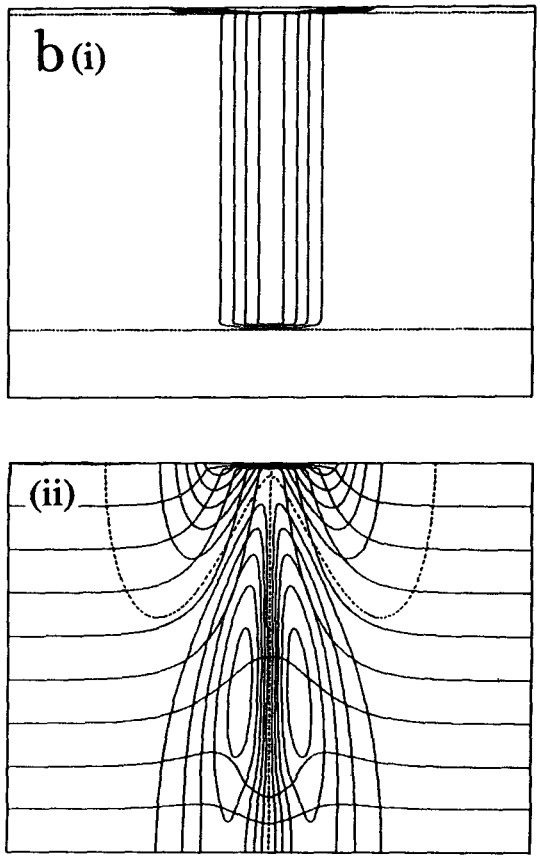

FIG. 5b. The idealized potential vorticity distribution $\tilde{Q}$ shown in (i) is inverted. It is identical to that shown in (a) (i) apart from the insertion of a sheet of positive potential vorticity just below the surface, of a magnitude such that the total potential vorticity anomaly integrated over the whole volume is zero. The inversion is carried out as before but now, unlike in (a), upper and lower boundaries are assumed to be isothermal. The inverted temperature and velocity fields are almost identical to those seen in (a); note in particular, however, that now the isotherms do not outcrop at the surface. Contour intervals as in Fig. 5a.

streamfunction for the geostrophic flow, $\sigma' = (-\rho_s f_0/g)(\partial\psi/\partial z)$ is the potential density anomaly, and $N^2 = (-g/\rho_s)(d\sigma_0/dz)$ is a measure of the strength of the reference stratification with ρ_s a constant reference measure of density. In the case of our numerically produced geostrophically adjusted plume (see Fig. 3a) we have $L \sim 2$ km, $V \sim 10^{-1}$ m s^{-1}, $H \sim 1$ km, and $N^2 = 5 \times 10^{-8}$ s^{-2}, so that Ro has a value of 0.5, Ri = 5, and $(\text{Ri Ro})^{-1} = 0.4$. We can therefore see that this situation is at the very limit of applicability of the quasigeostrophic approximation.

Motivated by the previous analysis we define a modified quasigeostrophic potential vorticity distribution [analogous to Eq. (4)]

$$\tilde{q} = q + \gamma\delta(z-), \tag{11}$$

where q is given by (10) and γ is the strength of the quasigeostrophic potential vorticity sheet that will represent surface anomalies. The magnitude of γ, which has units of velocity, can be deduced by invoking the constraint, analogous to (8), that

$$\int \tilde{q}dV \equiv 0. \tag{12}$$

The boundary conditions used to invert the modified PV (11) is that the upper and lower boundaries are isopycnal surfaces, so that $\partial\psi/\partial z = 0$ there.

Combining (10), (11), and (12), we deduce that the sheet of potential vorticity must have a strength (as first shown by Bretherton 1966)

$$\gamma = \frac{gf}{\rho_s}\frac{\sigma'_{\text{surface}}}{N^2}, \tag{13}$$

where $\sigma'_{surface}$ is the surface potential density anomaly, which is being replaced by the potential vorticity sheet. Thus, if the surface is cold γ is positive; if it is warm γ is negative. Hence, a balanced vortex created by convective overturning can be idealized by a negative PV anomaly in the interior, associated with the reduction of stratification in the mixed water column, and a positive potential vorticity anomaly just below the surface, representing the cold surface. The total, vertically integrated anomaly is identically zero, and the strength of the anomaly in the quasigeostrophic limit is directly proportional to the surface potential density anomaly.

3. A heton model of geostrophically adjusted plumes

To study the interaction of a cluster of mature plumes, we use a point-vortex heton model, in which the potential vorticity structure of individual plumes is represented by a positive anomaly in the upper layer of a two-layer model coupled with a negative anomaly in the lower layer, but now within a quasigeostrophic framework. A two-layer formulation is chosen because it is the simplest capable of representing the PV structure of the baroclinic vortex; the cold surface is equivalent to a source of anomalously high PV inducing cyclonic flow in the upper layer, while the stratification over the interior of the vortex is very weak and so anomalously low in PV, inducing anticyclonic flow in the lower layer.

a. Formulation

The two-layer model of Hogg and Stommel (1985a) represents the effects of the surface density anomalies implicitly by working, as in all layer quasigeostrophic models, directly in terms of $\tilde{q}$ rather than representing interior q and surface density anomalies separately. Hence, the appropriate form of the $\tilde{q}$ in the two-layer model can be inferred directly from (10), using the boundary condition $\partial\psi/\partial z = 0$ [together with (11) and (12)];

$$\tilde{q}_1 = \nabla^2\psi_1 - F(\psi_1 - \psi_2), \tag{14a}$$

$$\tilde{q}_2 = \nabla^2\psi_2 + F(\psi_1 - \psi_2), \tag{14b}$$

where

$$F = \frac{f_0^2}{N^2h^2} = \frac{4}{\pi^2 L_\rho^2},$$

$L_\rho = NH/(\pi f_0)$ is the Rossby radius of deformation, $h = H/2$ is the depth of one layer, and H is the total depth of the model (see Fig. 6a). The stretching terms represent the deviation of the interface between the two layers from its reference depth, and hence also measures the density anomaly at middepth. The PV distribution in the upper layer can be considered to represent the effect of the cold surface while the lower layer PV represents the PV in the interior of the column.

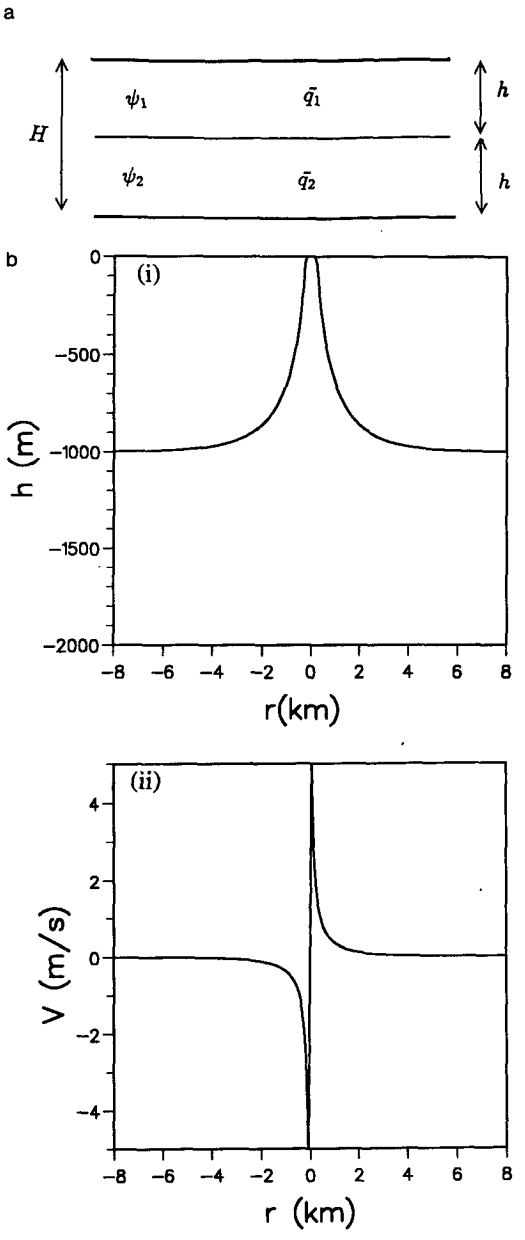

FIG. 6. (a) A schematic diagram showing the vertical structure of the two-layer quasigeostrophic model. The layer depths, h, are equal with $F = 4/(\pi^2 L_\rho^2)$. Point vortices of equal and opposite strength in the two layers induce the baroclinic vortex shown in (b). (b) The layer depths [as given by Eq. (18c)] and upper-layer azimuthal velocity fields [Eq. (18b)] induced by a single cold heton with equal but opposite vortex strengths in each layer. The strength of the point vortex is $s = 0.6\pi\lambda^2 f$ and $\lambda = 1.6$ km. Each of the two layers is 1 km deep and the reference stratification is $N^2 = 5 \times 10^{-8}$ s^{-2}. The velocity at a radius of λ is 10 cm s^{-1}. A population of hetons of this strength is used in the reference experiment of section 4a.

To satisfy the constraint (12) we require that, since our layers are of equal depth,

$$\tilde{q}_1 + \tilde{q}_2 = 0. \tag{15}$$

We suppose that the convectively formed vortex has a cold core of the order of the Rossby radius of deformation, so that viewed on the large scale they appear as delta functions of potential vorticity and coldness. We therefore represent each baroclinic vortex by a vertically aligned pair of point vortices of equal but opposite strength, to ensure that (15) is satisfied. Thus, the potential vorticity structure of each plume is idealized in the two-layer model as

$$\tilde{q}_1 = s\delta(\mathbf{r} - \mathbf{r}_0), \tag{16a}$$

$$\tilde{q}_2 = -s\delta(\mathbf{r} - \mathbf{r}_0), \tag{16b}$$

where s is the strength of the point vortex.

Inverting equations (14) for a potential vorticity distribution of the form given in (16), as shown, for example, by Hogg and Stommel (1985a), we find the streamfunction at a point $\mathbf{r}$ due to a vortex i, of strength s_i situated at the point $\mathbf{r}_i$, is

$$\psi = \frac{s_i}{2}\left[\ln(r) - K_0\left(\frac{r}{\lambda}\right)\right] \tag{17a}$$

in the layer of the vortex i, and

$$\psi = \frac{s_i}{2}\left[\ln(r) + K_0\left(\frac{r}{\lambda}\right)\right] \tag{17b}$$

in the layer not containing the vortex i. Here r is the distance of the point in question from the vortex $|\mathbf{r} - \mathbf{r}_i|$, $\lambda = 1/\sqrt{2F} = L_\rho(\pi/\sqrt{8})$ and $K_0(x)$ is the modulated Bessel function of zeroth order. Differentiating (17) to find the azimuthal velocity V_θ, we obtain

$$V_\theta = \frac{s_i}{2}\left[\frac{1}{r} + \frac{1}{\lambda}K_1\left(\frac{r}{\lambda}\right)\right] \tag{18a}$$

in the layer of the vortex i, and

$$V_\theta = \frac{s_i}{2}\left[\frac{1}{r} - \frac{1}{\lambda}K_1\left(\frac{r}{\lambda}\right)\right] \tag{18b}$$

in the other layer. The velocity field induced in the layer of the point vortex therefore tends to s/r at small r, while the velocity field induced in the opposite layer tends to zero. At large r, both fields tend to $(1/2)s/r$. For small r, therefore, the interaction between two vortices in the same layer is much stronger than the interaction between two vortices in opposite layers. The deformation radius λ determines the effective range of the vortex; interaction vortices only "feel" one another at separations of a few λ.

If we sum to find the combined effect of the two vortices of equal and opposite strength that make up a heton, we find

$$V_{1\theta} = \frac{|s|}{\lambda}K_1\left(\frac{r}{\lambda}\right),$$

$$V_{2\theta} = -\frac{|s|}{\lambda}K_1\left(\frac{r}{\lambda}\right),$$

where $V_{n\theta}$ refers to the velocity in layer n. There is no barotropic flow induced.

The height perturbation of the interface η between the two layers, is related to the streamfunction through $\eta = (f/g')\psi$ and is given by

$$\eta = \frac{f}{g'}|s|K_0\left(\frac{r}{\lambda}\right), \tag{18c}$$

where $g' = N^2H$ is the reduced gravity.

In Fig. 6b, we plot the interface height and azimuthal velocity field induced by a single cold heton; a quasigeostrophic representation of the primitive equation baroclinic vortex is shown in Fig. 3. Note that the interface domes up toward the surface; there is cyclonic vorticity in the upper layer, anticyclonic vorticity in the lower layer.

If a heton is tilted such that a finite horizontal separation Δr exists between the two vortices, then the heton will self-propagate at a velocity

$$|s|\left[\frac{1}{\Delta r} - \frac{1}{\lambda}K_1\left(\frac{\Delta r}{\lambda}\right)\right]$$

in a direction perpendicular to the line joining the vortices. This propagation mechanism leads to the transport of heat, since the heton carries with it a finite (anomaly) of thermal energy. Finally, several hetons of the same sign, when clustered together on scales on or less than λ, will behave as an "extended heton"—a baroclinic vortex of finite horizontal extent with similar properties to a single heton. This extended heton is the quasigeostrophic analog of the "cone" discussed in JM.

b. Heton strength and creation rate

Since the density anomaly at the interface is directly proportional to the stretching terms in (14a) and (14b), by integrating over all space we can deduce that each heton carries with it a finite density anomaly, most of which is concentrated in a region of $\sim 2L_\rho$ in diameter:

$$\int_\infty \sigma' dA = -\frac{\rho_s N^2 h}{gf}s = \frac{\rho_s \pi^2 L_\rho^2}{4gh}fs. \tag{19}$$

This facilitates an estimate of the strength of a heton if it is to represent the average density anomaly σ_{av} averaged over an area of radius L_ρ of our numerically generated convection plume. Equation (19) suggests that

$$s \approx \frac{4g}{\pi}\frac{\sigma_{\text{av}}}{\rho_s}\frac{h}{f}. \tag{20}$$

From (19) the total deficit of thermal energy associated with one heton can be evaluated thus:

$$E = C_w \rho h \int_\infty T' dA = \frac{\rho_s C_w \pi^2 L_\rho^2}{4g\alpha}fs, \tag{21}$$

where α is the coefficient of thermal expansion of water and C_w is the specific heat of water.

NUMERICAL ESTIMATES

Examination of the structure of the geostrophically adjusted plume simulated by our primitive equation model (see Fig. 3), in which the ambient Rossby deformation radius $L_\rho = (NH)/(\pi f)$ has a magnitude of 1.42 km, reveals the density anomaly associated with the cold water plume to be about 3.7×10^{-3} kg m^{-3}, corresponding to a temperature deficit of 0.018 K, averaged over a disk of radius L_ρ to a depth of 1 km. Substituting these values into the expression for heton strength, Eq. (20) gives an estimate of $s = 4.75 \times 10^2$ m^2 s^{-1}. This is equivalent to an average PV anomaly associated with the heton of $\hat{q}_{\text{het}} = .6f$ over a disk of radius λ and, from (21), a deficit of thermal energy of 0.48×10^{15} J. (Here, $\hat{q}_{\text{het}}$ gives the equivalent average potential vorticity over a disk of radius λ; $s = \hat{q}_{\text{het}}\pi\lambda^2$.)

Now if the large-scale heat loss is $\mathscr{H}$ (W m^{-2}) over a disk of area $\mathcal{A}$, then the rate of generation of hetons $\partial\mathcal{N}/\partial t$, each with a deficit of thermal energy E, is

$$\frac{\partial \mathcal{N}}{\partial t} = \frac{\mathscr{H}\mathcal{A}}{E}. \tag{22}$$

Thus after a time T, a number $\mathscr{H}\mathcal{A}T/E$ of hetons will have been generated and their average separation will be $(E/\mathscr{H}T)^{1/2}$. If the large-scale heat loss is 800 W m^{-2} and the radius of the convection site is 8 km, as in the numerical experiments of JM, then 33 hetons, each with a thermal deficit of 0.48×10^{15} J, will be generated in one day and their average separation at one day will be $\sim$2.4 km, of the order of the radius of deformation. Thus, we can expect that the baroclinic point vortices will strongly interact with one another after only one day.

One may also enquire into the strength of the rim current around the convection site induced by hetons of this strength and number. The average potential vorticity anomaly $\hat{q}$ associated with $\mathcal{N}$ point vortices over an area $\mathcal{A}$ is

$$\int q dA = \hat{q}\mathcal{A} = \mathcal{N}s, \tag{23}$$

where s is the strength of a heton, and $\mathcal{N}$ is the total number of hetons in the disk of area $\mathcal{A}$. The maximum shear of the rim current is related to $\hat{q}$, thus (from Pedlosky 1985):

$$\Delta V \sim \hat{q}\lambda, \tag{24}$$

and so, combining Eqs. (23) and (24) we obtain

$$\Delta V \sim \frac{s\lambda\mathcal{N}}{\mathcal{A}}. \tag{25}$$

A total of 33 hetons of strength $\hat{q}_{\text{het}} = 0.6f$ in a disk of radius 8 km where the ambient radius of deformation is 1.42 km induces a rim current of 0.12 m s^{-1}, roughly in accord with the explicit numerical simulation presented in section 7 of JM.

c. *Rate of generation of potential vorticity*

We can obtain the quasigeostrophic potential vorticity equation by integrating, in turn, Eq. (2) over each quasigeostrophic layer of depth h thus,

$$h\left(-\frac{d\sigma_0}{dz}\right)\left(\int \frac{\partial}{\partial t}\tilde{q}dA + \int \nabla\cdot(\tilde{q}\mathbf{v})dA\right) = \int g^{-1}B_{\text{int}} f dA, \tag{26}$$

where B_{int} is the buoyancy forcing at the interface between the two layers, ω has been replaced by f, and we have made use of (9). Expressing B_{int} in terms of the divergence of the heat flux:

$$B_{\text{int}} = \frac{g\alpha\mathscr{H}_{\text{int}}}{C_w h},$$

where $\mathscr{H}_{\text{int}}$ is the rate of cooling per unit area, Eq. (26) becomes for each layer:

$$\frac{D}{Dt}\tilde{q}_{\text{top}} = -\frac{g\alpha f\mathscr{H}_{\text{int}}}{\rho_s C_w h^2 N^2}, \tag{27}$$

$$\frac{D}{Dt}\tilde{q}_{\text{bottom}} = \frac{g\alpha f\mathscr{H}_{\text{int}}}{\rho_s C_w h^2 N^2}, \tag{28}$$

in which D/Dt is the substantial derivative. The upper-layer PV anomaly is positive if there is cooling ($\mathscr{H}_{\text{int}} < 0$), and the rate of change of potential vorticity is equal and opposite in the two layers. There is no net change in $\tilde{q}$ over the fluid column, in complete analogy with Eq. (8).

The total rate of generation of hetons due to cooling confined to a disk of surface area $\mathcal{A}$ is, therefore, integrating (26) over all space and using Eq. (23)

$$\frac{\partial \mathcal{N}_{\text{tot}}}{\partial t} = \frac{g\alpha f\mathscr{H}_{\text{int}}}{\rho_s C_w h^2 N^2}\frac{\mathcal{A}}{s}, \tag{29}$$

where $\mathcal{N}_{\text{tot}}$ is the total number of hetons and s is the strength of a single vortex. This is precisely the same expression as that deduced earlier from energetic considerations [Eq. (22)] as can be seen by making use of Eq. (21).

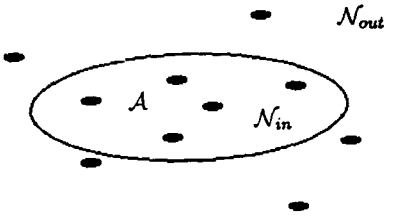

FIG. 7. A schematic diagram showing $\mathcal{N}_{\text{in}}$ hetons within the convective disk of area $\mathcal{A}$ and $\mathcal{N}_{out}$ hetons outside the disk. The total number of hetons $\mathcal{N}_{\text{tot}} = \mathcal{N}_{\text{in}} + \mathcal{N}_{\text{out}}$ increases at a rate given by Eq. (29).

Integrating (26) over the area $\mathcal{A}$ we have

$$\frac{\partial \mathcal{N}_{\text{in}}}{\partial t} + \frac{\partial \mathcal{N}_{\text{out}}}{\partial t} = \frac{\partial \mathcal{N}_{\text{tot}}}{\partial t}, \tag{30}$$

where each term in (30) corresponds to respective terms in (26), $\mathcal{N}_{\text{in}}$ denotes the number of hetons within the area $\mathcal{A}$, $\mathcal{N}_{\text{out}}$ is the number outside, and $\mathcal{N}_{\text{tot}}$ is the total number increasing at the rate (29) (see Fig. 7).

In the numerical experiments described in section 4 we will use (29) to prescribe the rate at which hetons are introduced into the convection site exposed to surface cooling. We assume that the time over which downwelling occurs is much shorter than the time scale of the interactions between the vortices, so that the formation of a heton is, in effect, instantaneous.

4. Experiments with the heton model

Our numerical experiments assume a constant cooling of 800 W m^{-2} over a disk of diameter 16 km (or, equivalently, 10λ) consistent with the explicit calculations of JM. Observations (for example, see Schott and Leaman 1991) suggest that cooling rates can rise to 1000 W m^{-2} and persist for ~2 days, falling to a background value of ~200 W m^{-2}, which may last for many weeks. Cooling at a rate of 800 W m^{-2} creates hetons of strength $\hat{q}_{\text{het}} = 0.6f$ at a rate of 33 per day as

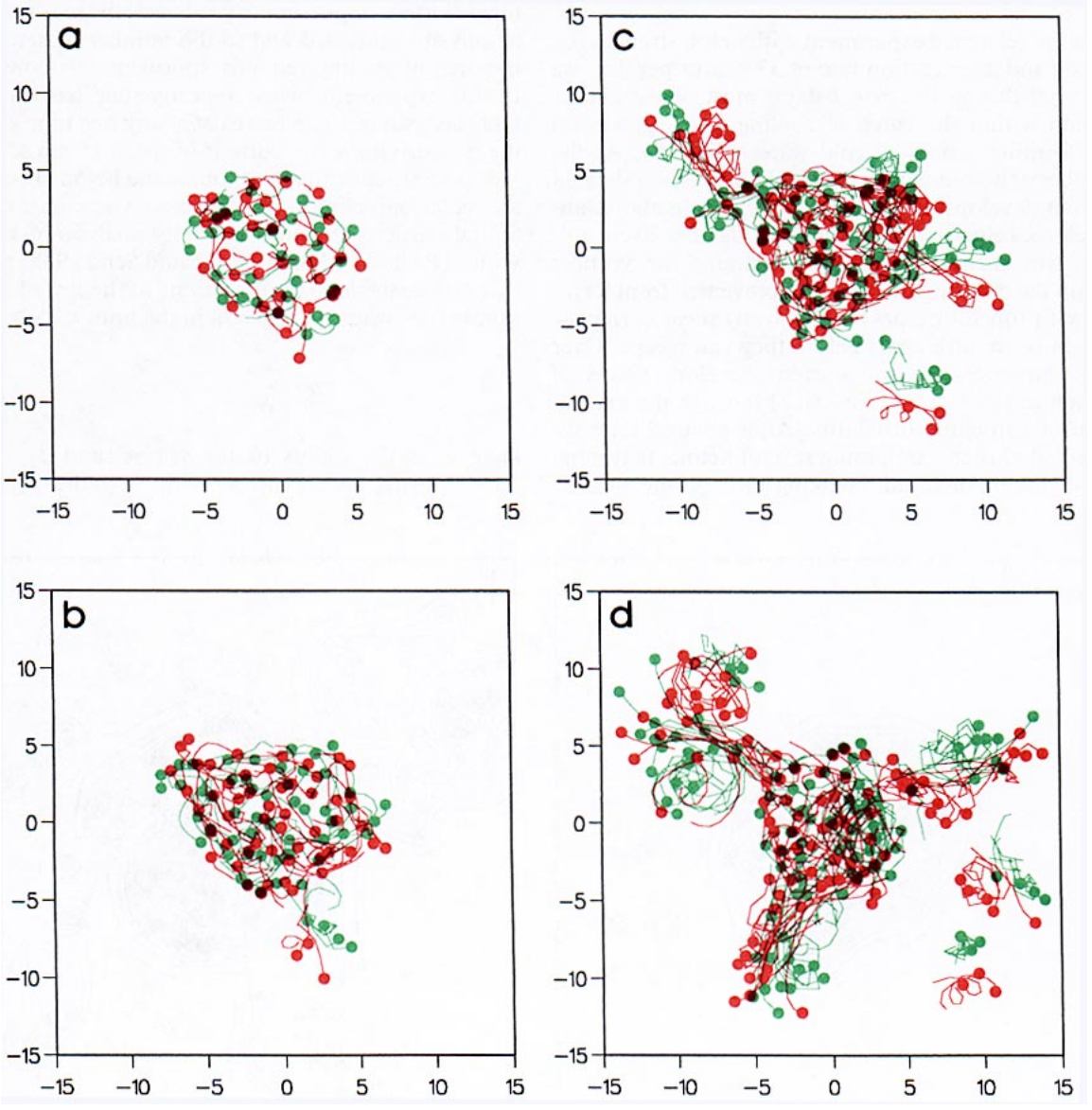

FIG. 8. Four pictures charting the development of an evolving cluster of hetons in the reference experiment. Each picture shows the trajectories of the hetons over a period of 0.6 days: (a) 0.6–1.2 days, (b) 1.2–1.8 days, (c) 1.8–2.4 days, (d) 2.4–3.0 days. The trajectories of the upper-layer vortices are shown in green, while those of the lower-layer vortices are shown in red. The horizontal scale is presented in units of λ and the hetons are introduced over a disk of radius 5λ.

previously deduced. They are introduced with random initial (Cartesian) coordinates but as described in section 4a, we impose the additional constraint that newly created hetons must be introduced at a distance $\geq \lambda$ from preexisting hetons. This prevents dense local clusters from forming. The vortex positions are stepped forward in time using the velocity fields (18) employing a fourth-order Runge–Kutta algorithm with a time step of 20 minutes. As described in 4c, further numerical experiments have been performed with different values of heton strength and alternative recipes for introducing the hetons, to study the sensitivity of the resulting behavior to these factors.

a. *The behavior of the convective plumes in the reference experiment*

In the reference experiment with heton strength $\hat{q}_{het} = 0.6f$ and a generation rate of 33 hetons per day, we find that during the first 2 days, most of the hetons remain within the patch of cooling (see Fig. 8a and 8b) forming a pool of cold water (Fig. 9a). As the number of hetons within the patch increases, a sheared current develops around the rim, cyclonic above, anticyclonic below, reaching a magnitude of ~ 20 cm s^{-1}. This rim current effectively constrains the vortices within the disk. Initially they are prevented from forming self-propelling pairs by this strong shear current—any pairs are torn apart before they can escape. Over time, however, the rim current develops waves of modenumber 4–5 (see Fig. 8b,c) through the mechanism of baroclinic instability. After about 2 days we see tilted clusters containing several hetons that burst out of the main cloud, breaking through the sheared rim current (Fig. 8c). The convection site therefore breaks up into several smaller tilted clusters that propagate outwards, resulting in a fall in the number of hetons in the patch where cooling is occurring (see Fig. 10 which plots the number of hetons inside and outside the convection disk as a function of time). The heton clusters continue to travel outwards (Fig. 8d), carrying cold water far from the area of cooling (Fig. 9b). These extended hetons, clumping together on the radius of deformation scale, are very efficient at fluxing heat laterally into the cooling area (see section 4b).

As time progresses and the hetons disperse, the magnitude of the rim current diminishes, so that it is easier for subsequent groupings to move outwards. Ultimately a steady state is reached (see Fig. 10) in which the flux of hetons out of the area of cooling, in the form of tilted clusters, approximately balances the rate at which hetons are generated and so the number of hetons in the area of cooling remains approximately constant. In this experiment, when a steady state has been established, some 30 hetons exist at any one time within the disk driving a rim current of speed 15 cm s^{-1}.

It is instructive to approximate the heton cluster by a circular baroclinic vortex of piecewise constant potential vorticity $\hat{q}$. Linear stability analysis of such a vortex (Pedlosky 1985; Helfrich and Send 1988) shows that it is unstable to perturbations of the rim of mode number m, where m is given, in the limit $r_o/\lambda \geq 2$, by

$$m \leq \frac{r_o}{\lambda}, \quad m \neq 1. \tag{31}$$

Here r_o is the radius of the vortex, and $\lambda = (\pi/\sqrt{8})L_\rho$. Any such vortex with a radius greater

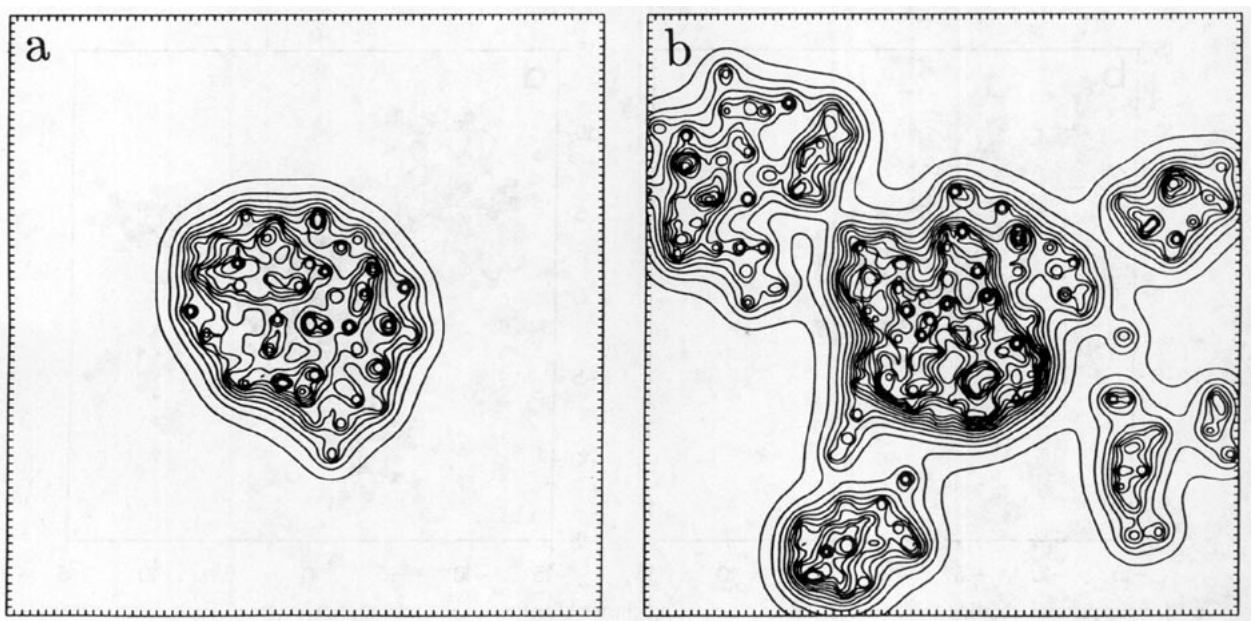

FIG. 9. Horizontal maps of the temperature anomaly at a depth of 1 km at (a) day 1 and (b) day 3 in the reference experiment. The contour interval is .005 K.

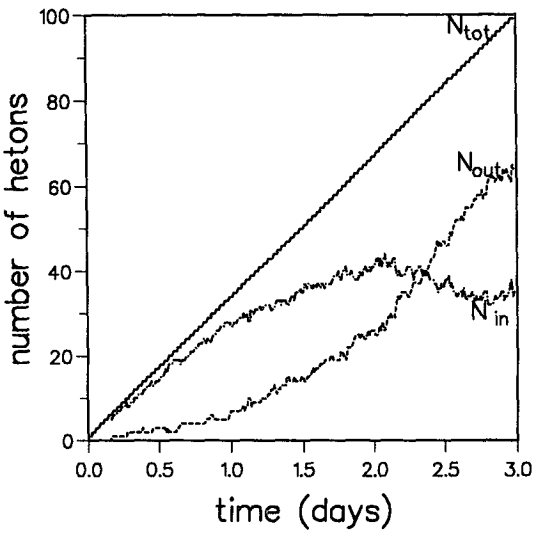

FIG. 10. The evolution in time of $\mathcal{N}_{tot}$, $\mathcal{N}_{in}$, $\mathcal{N}_{out}$ in the reference experiment.

than 2λ or $(\pi/\sqrt{2})L_\rho$ will therefore be linearly unstable. A heton cluster of radius $r_0 = 5\lambda$, where $\lambda = 1.6$ km, would therefore be expected to be unstable to all modes of modenumber $m \leq 5$, and the larger modenumbers will have the fastest growth rates. We do in fact observe instability of mode number 4 or 5, as expected (see Figs. 8b,c and 9c).

The growth rate for the two-layer piecewise-constant baroclinic vortex is given by Eq. (3.10) of Pedlosky (1985):

$$c_i m = \hat{q} m \left[\frac{I_m\left(\frac{r_0}{\lambda}\right) K_m\left(\frac{r_0}{\lambda}\right)}{2m} \times \left(1 - 2mK_1\left(\frac{r_0}{\lambda}\right) I_1\left(\frac{r_0}{\lambda}\right)\right) \times \left(\frac{K_1\left(\frac{r_0}{\lambda}\right) I_1\left(\frac{r_0}{\lambda}\right)}{K_m\left(\frac{r_0}{\lambda}\right) I_m\left(\frac{r_0}{\lambda}\right)} - 1 \right) \right]^{1/2}. \quad (32)$$

For the fastest growing mode in the range $r_0/\lambda \geq 2$, the numerical factor in the square brackets asymptotes to $(0.1/m)^2$, and so (32) simplifies to

$$c_i m \approx 0.1\hat{q}. \quad (33)$$

The appropriate $\hat{q}$ for our reference numerical experiment can be found thus,

$$\hat{q} = \frac{(s\mathcal{N}_{in})_{max}}{\mathcal{A}}, \quad (34)$$

where $(\mathcal{N}_{in})_{max}$ is the maximum number of hetons in the cooling area. We find $\hat{q}$ to have a value $0.95f$, resulting in an expected baroclinic growth rate of about 1 day. This agrees well with the observed breakup at our cold chimney in about 2 days, since it takes 1 day to reach $(\mathcal{N}_{in})_{max}$.

b. *The thermodynamics of the convective patch*

We saw earlier how temperature anomalies can be represented by a subsurface sheet of potential vorticity, and how explicit cooling can be parameterized by a rate of generation of hetons. We can extend these ideas to investigate the thermodynamics and heat balance of our cloud of hetons. Since from (21) each heton carries with it a finite heat anomaly, the thermodynamic equation, integrated over the area of cooling, can be written as [using Eqs. (22) and (30)]

$$E\frac{\partial \mathcal{N}_{in}}{\partial t} + E\frac{\partial \mathcal{N}_{out}}{\partial t} = \mathscr{K}\mathcal{A}, \quad (35)$$

where E is the heat associated with a single heton, taken to be -0.48×10^{15} J in our reference experiment. The rate at which heat is fluxed into the area of cooling $\mathcal{A}$ [the second term on the left-hand side of (35)] can be inferred from the behavior of our cloud of hetons. In particular, when a quasi-equilibrium state is reached, such that $\partial \mathcal{N}_{in}/\partial t = 0$, the rate at which heat is fluxed into the area of cooling must be equal to the rate of heat loss at the surface. For a rate of cooling of 800 W m^{-2} over an area of diameter 16 km as here, the heat must be fluxed in at a rate of 1.6×10^{11} W. If each heton carries with it an energy deficit of -0.48×10^{-15} J, we require $\sim$30 hetons per day to cross the bounday of the convective disk—this is just the slope of the $\mathcal{N}_{out}$ curve at large times shown in Fig. 10.

The cloud of hetons therefore goes through two distinct stages. Initially there is little lateral heat flux out of the area $\mathcal{A}$ and the surface cooling increases the local temperature anomaly, leading to the formation of a cold pool of water. Later on, by about two days, a quasi-steady state arises in which the temperature in the area $\mathcal{A}$ remains approximately constant, and surface cooling is balanced by a highly efficient organisation of the hetons, fluxing heat laterally in motion systems with a scale of the radius of deformation, through the mechanism of baroclinic instability.

c. *Sensitivity to initial heton distribution*

A number of experiments have been performed employing various recipes for the introduction of hetons parameterizing the patchiness of open-ocean deep convection. In the reference experiment, the hetons had an equal probability of being generated anywhere over the cooling patch, but with the added restriction that there must be a minimum separation of λ between any heton introduced and preexisting hetons. If this constraint is relaxed and the initial coordinates of the heton are chosen completely randomly, as in the sim-

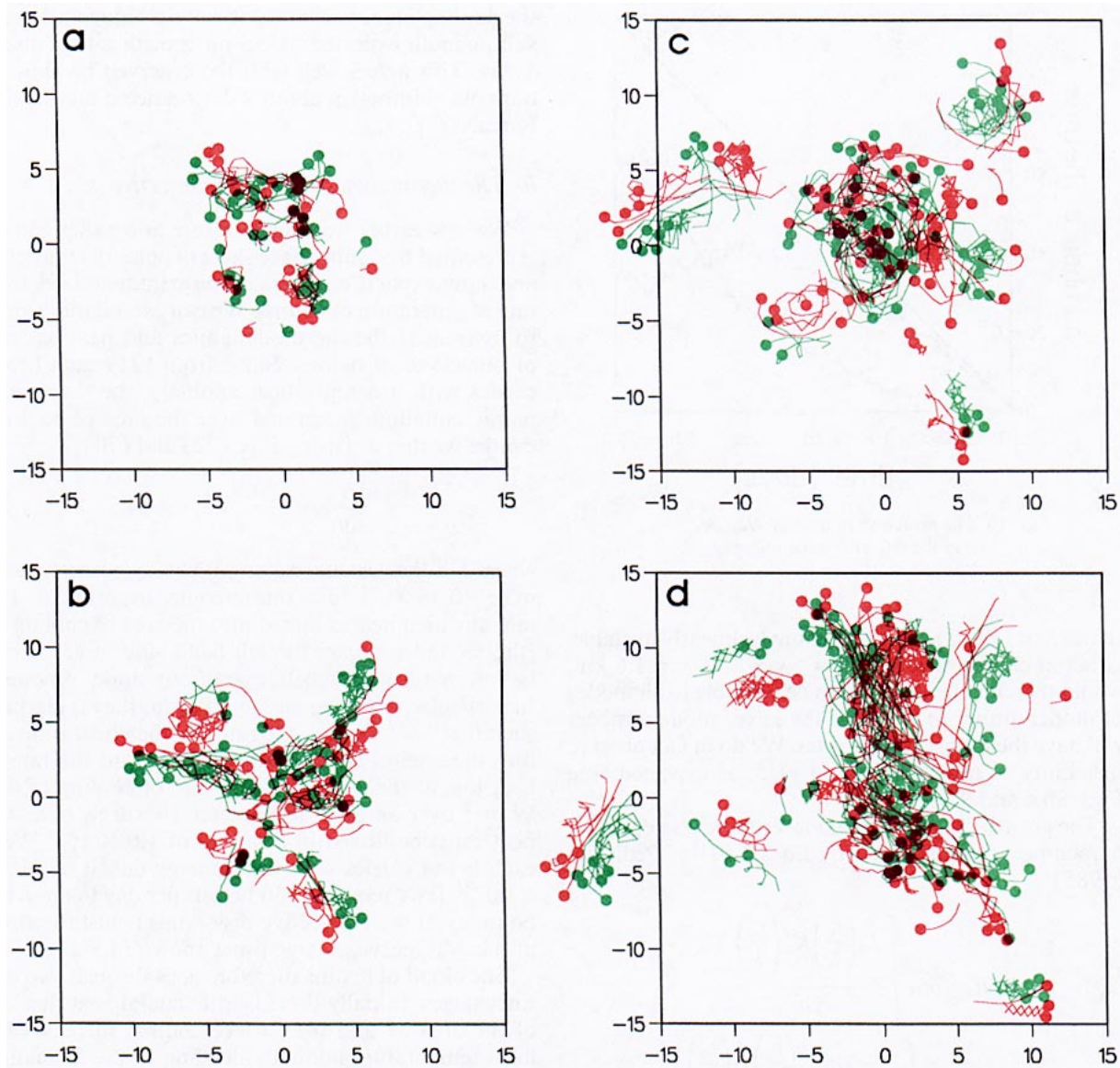

FIG. 11. Four pictures charting the development of an evolving cluster of hetons introduced completely randomly in space over the convective disk at a rate given by the large-scale heat loss. Each picture shows the trajectories of the hetons over a period of 0.6 days: (a) 0.6–1.2 days, (b) 1.2–1.8 days, (c) 1.8–2.4 days, (d) 2.4–3.0 days. The trajectories of the upper-layer vortices are shown in green, while those of the lower-layer vortices are shown in red. The horizontal scale is presented in units of λ and the hetons are introduced over a disk of radius 5λ.

ulation presented in Fig. 11, the distribution of hetons within the cooling area can become less uniform, and there will be local clustering of hetons within the patch. These local clusters, when tilted, have a sufficiently large self-propulsion velocity to break through the rim current, allowing the patch to break up more quickly via lower modes. For example, in Fig. 11 we clearly see a mode 3 instability after $1\frac{1}{2}$ days.

Experiments were carried out in which the uniform distribution of the hetons within the patch was relaxed still further; if hetons are introduced with a greater frequency in the central part of the patch then, since the fastest growing baroclinic mode has a modenumber directly proportional to the ratio between the cluster radius and λ, the preferred mode number for breakup of the cluster is reduced still further. In Fig. 12, where the vortices were introduced using a recipe that preferentially placed them near the center of the disk (random values of radius and azimuth were chosen), a mode 2 instability develops reminiscent of the hydrothermal plume experiments of Helfrich and Battisti (1991); the patch of cold water "fills out" from the center until (31) is satisfied, leading to the growth of the lowest mode of instability.

d. Sensitivity to heton strength

We have performed a number of experiments enquiring into the sensitivity of our results to heton strength. Since the rate of increase of potential vorticity within the cooling area is dependent only on the rate of cooling [see Eq. (27)] this will be a constant if $\mathscr{K}$ is held constant; however, the extent to which the potential vorticity is discretized, when viewed from the large scale, will depend on the assumed strength of the individual hetons. Intense hetons will result in a lower rate of heton production and vice versa, since the rate of heton generation is inversely proportional to the strength. For variations in the strength, $s = 0.6f\pi\lambda^2$, $0.79f\pi\lambda^2$, $0.95f\pi\lambda^2$, there is little qualitative difference in the behavior. All clouds break up at about 2 days and all reach a quasi-steady state in which, interestingly, similar values of average potential vorticity over the disk $\hat{q} = \mathscr{N}s/\mathscr{A}$ are found (see Fig. 13). This might be expected from baroclinic instability theory since (Pedlosky 1985) the growth rate of the instability is dependent only on the value of $\hat{q}$ and the radius of the patch.

There is, however, a notable difference when the heton strength is increased to very large values, such that the rate at which the hetons are generated for a given

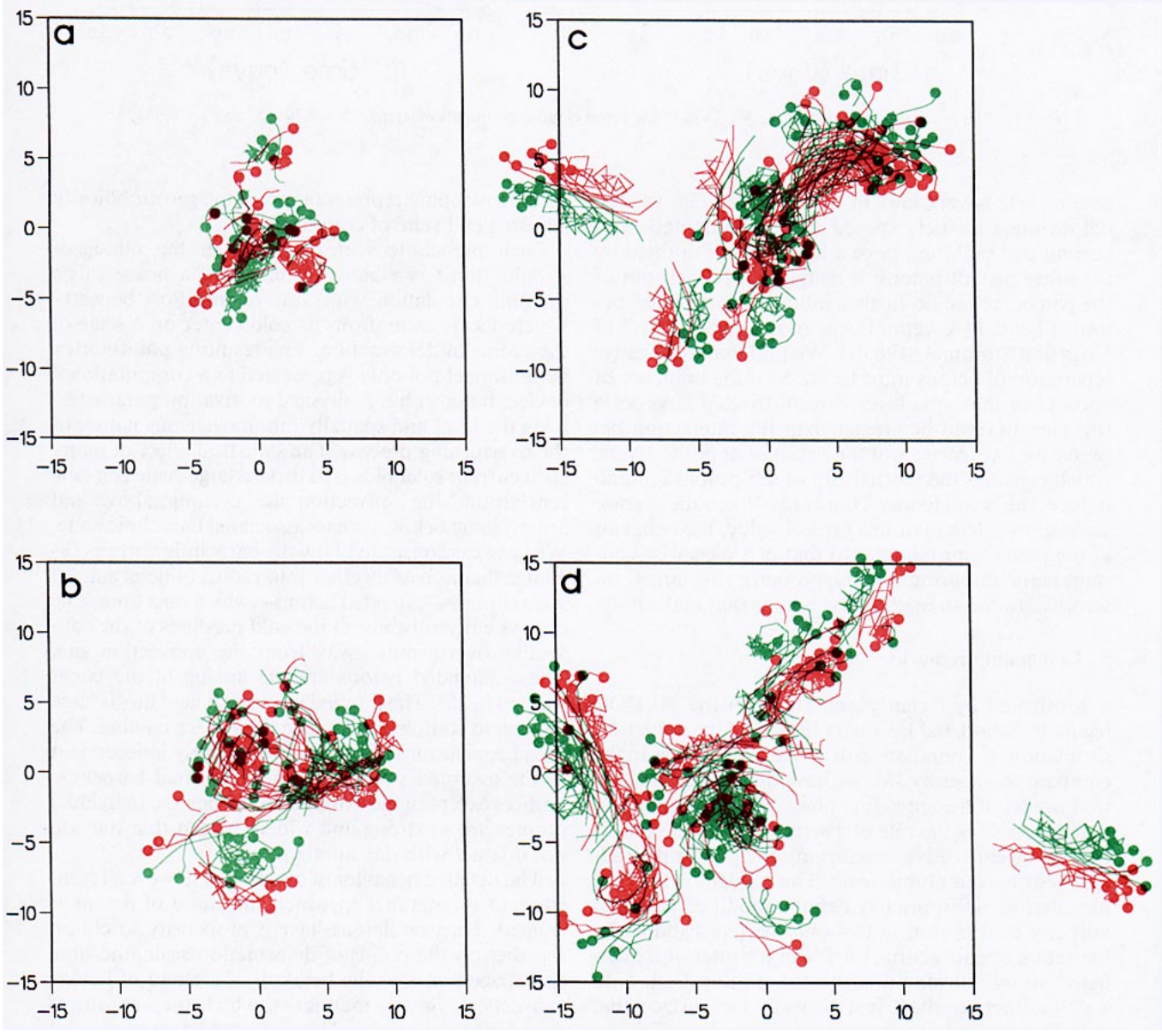

FIG. 12. Four pictures charting the development of an evolving cluster of hetons introduced at a constant rate, but now preferentially at the center of the convection disk. Each picture shows the trajectories of the hetons over a period of 0.6 days: (a) .6–1.2 days, (b) 1.2–1.8 days, (c) 1.8–2.4 days, (d) 2.4–3.0 days. The trajectories of the upper-layer vortices are shown in green, while those of the lower-layer vortices are shown in red. The horizontal scale is presented in units of λ and the hetons are introduced over a disk of radius 5λ.

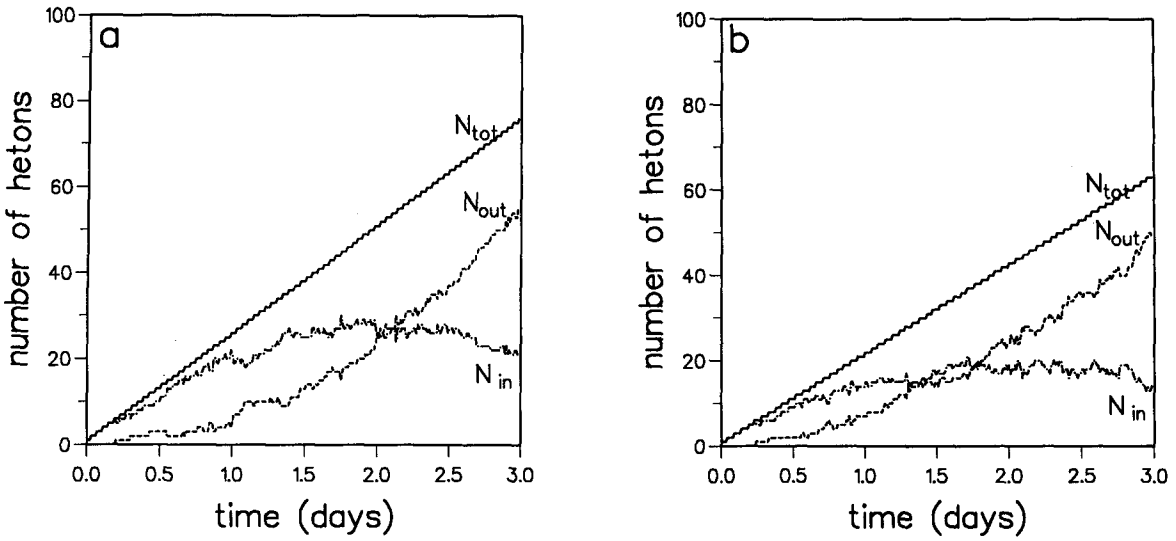

FIG. 13. The evolution in time of $\mathcal{N}_{tot}$, $\mathcal{N}_{in}$, $\mathcal{N}_{out}$ in the heton cloud experiments of strength $s = 0.79\pi f\lambda^2$ and $s = 0.95\pi f\lambda^2$.

cooling rate is very low. In this case (see Fig. 14) the hetons are so widely spaced that no systematic rim current can build up; once a heton has been tilted by the other distant hetons, it simply self-propels out of the patch, feeling no further influence from other hetons. Figure 14 is reminiscent of the "star-bursts" of Hogg and Stommel (1985b). We find that the average separation of hetons must be $\leqslant 2.5\lambda$ if the influence of vortices in the same layer, which drives a large-scale rim current, is to be greater than the interaction between the two vortices of the heton in opposite layers, which provides the mechanism of self-propulsion and induces the heton to travel outwards. When the average separation is less than this critical value, the behavior of the patch approximates to that of a piecewise-constant baroclinic vortex, whose properties are largely insensitive to the strength of the hetons that make it up.

5. Concluding remarks

Motivated by recent observations in the MEDOC region by Schott and Leaman (1991) and the numerical simulation of a population of convective plumes in the companion paper by JM, we have developed an idealized model of the spreading phase of deep convection that emphasizes the role of discrete baroclinic vortices formed by convective overturning and geostrophic adjustment on the plume scale. The model exploits the idea that an appropriately defined modified potential vorticity distribution $\tilde{Q}$ can only be redistributed by the action of convection; the PV of the interior is evacuated, as overturning destroys the stratification, onto a delta-function sheet just beneath the surface that represents the cold surface created by cooling. This device is used to parameterize the convective process and acts as a convenient bridge between the unapproximated equations summarized by (1) and a two-layer quasigeostrophic representation of the geostrophically adjusted end state of convection.

Each baroclinic vortex—which in the quasigeostrophic limit is a heton—consists of a near-surface cyclonic circulation with anticyclonic flow beneath, which decays away from its cold center on a scale of the radius of deformation. The resulting point-vortex heton model not only is presented as a computational device, but also has a physical motivation parameterizing the local and spatially inhomogeneous nature of the overturning process. The statistical effect of many such current solenoids is to drive a large-scale rim current around the convection site, cyclonic above and anticyclonic below, with its associated baroclinic zone. We have demonstrated how the baroclinic vortices organize themselves together into radius of deformation scale clumps—extended hetons—which on a time scale of days efficiently advect the cold products of the convective overturning away from the convection site. These extended hetons are the analog of the cones studied in JM. The implied horizontal heat flux is large enough to completely balance the surface cooling. The broad conclusions of our study are largely independent of the assumed strength of the individual baroclinic vortices except in the extreme limit when the individual plumes are so strong and widely spaced that they do not interact with one another.

The detailed behavior of our model, however, is sensitive to the manner in which the cloud of hetons is created. Because hetons have a propensity to clump together on the radius of deformation scale, the time and space scales of the breakup of a cloud of hetons can depend on the manner in which they are introduced into the model. Thus, an important avenue of research for the future is to develop an understanding of those factors that control the patchiness and organization of convective plumes on subgeostrophic scales.

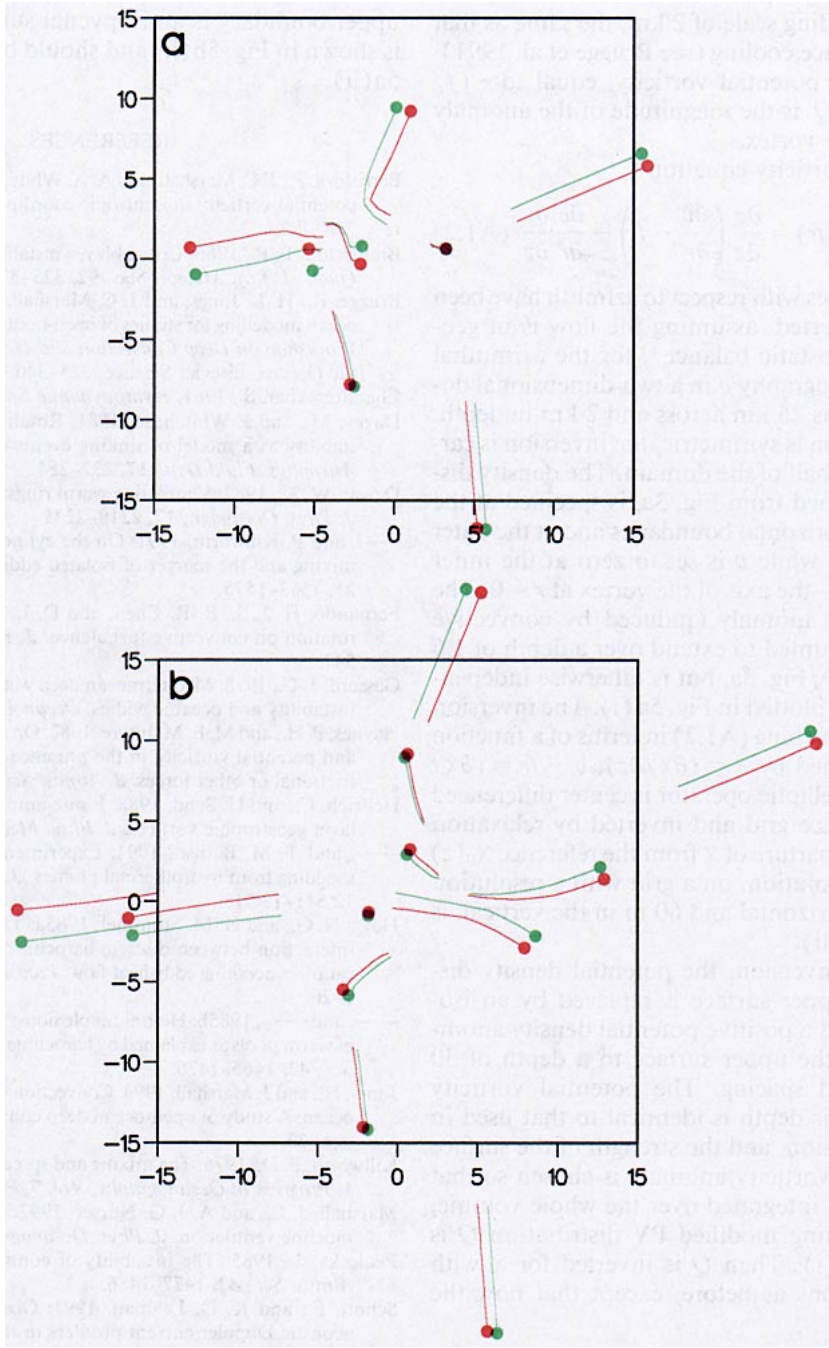

FIG. 14. The evolution of a cloud of hetons each of strength $s = 3.0\pi f\lambda^2$. (a) 0.6–1.2 days, (b) 1.2–1.8 days.

Acknowledgments. Support was provided by the Natural Environment Research Council of the United Kingdom and the NOAA Atlantic Climate Change Program. Alistair Adcroft kindly carried out the calculations described in the Appendix.

APPENDIX

Potential Vorticity Inversions

A two-dimensional potential vorticity inversion (r, z) is used to obtain the velocity and potential density fields of an axisymmetric baroclinic vortex from an idealized potential vorticity distribution. We assume that all fields are independent of azimuthal coordinate. The baroclinic vortex shown in Fig. 3 was induced by a pattern of cooling at the surface of a Gaussian form. For simplicity we assume that the potential vorticity anomaly induced by convective overturning has a similar spatial form

$$Q = Q_0 - Q' \exp\left[-\left(\frac{r}{b}\right)^2\right], \qquad \text{(A1.1)}$$

where b is an e-folding scale of 2 km, the same as that of the applied surface cooling (see Brugge et al. 1991), Q_0 is the ambient potential vorticity, equal to $-(f/\rho_s)(\partial\sigma_0/\partial z)$, and Q' is the magnitude of the anomaly at the center of the vortex.

The potential vorticity equation

$$\rho_s Q = -J(\sigma, v - fr) = \frac{\partial\sigma}{\partial z}\left(\frac{\partial v}{\partial r} - f\right) - \frac{\partial\sigma}{\partial r}\frac{\partial v}{\partial z} \quad \text{(A1.2)}$$

(where all derivatives with respect to azimuth have been set to zero) is inverted, assuming the flow is in geostrophic and hydrostatic balance[2], for the azimuthal current v and hydrography σ in a two-dimensional domain of dimensions 25 km across and 2 km in depth. Since the circulation is symmetric, the inversion is carried out over only half of the domain. The density distribution, as obtained from Fig. 3a, is specified at the upper and lower horizontal boundaries and at the outer vertical boundary, while v is set to zero at the inner vertical boundary—the axis of the vortex at $r = 0$. The potential vorticity anomaly (induced by convective overturning) is assumed to extend over a depth of 1.6 km, as suggested by Fig. 3a, but is otherwise independent of height; it is plotted in Fig. 5a (i). The inversion is carried out by couching (A1.2) in terms of a function χ, where χ is defined by $\sigma = (\partial\chi/\partial z)$; $v - fr = (\partial\chi/\partial r)$. The resulting elliptic operator is center differenced on a finite-difference grid and inverted by relaxation for $\delta\chi(r, z)$, the departure of χ from the reference $\chi_0(z)$ fixed by Q_0. The solution, on a grid with a resolution of 192 m in the horizontal and 60 m in the vertical, is shown in Fig. 5a (ii).

In the second inversion, the potential density distribution at the upper surface is replaced by an isopycnal surface, and a positive potential density anomaly is inserted at the upper surface to a depth of 30 m—half of a grid spacing. The potential vorticity anomaly below this depth is identical to that used in the previous inversion, and the strength of the surface positive potential vorticity anomaly is chosen so that the total anomaly, integrated over the whole volume, is zero. The resulting modified PV distribution $\tilde{Q}$ is shown in Fig. 5b(i). Then $\tilde{Q}$ is inverted for χ with boundary conditions as before, except that now the upper boundary is an isopycnal surface. The solution is shown in Fig. 5b(ii) and should be compared to Fig. 5a(ii).

[2] For simplicity cyclostrophic terms have been neglected in our balance condition and r is assumed to be rectilinear.

REFERENCES

Berrisford, P., J. C. Marshall, and A. A. White, 1993: Quasigeostrophic potential vorticity in isentropic coordinates. *J. Atmos. Sci.*, **50,** 778–782.

Bretherton, F. P., 1966: Critical layer instability in baroclinic flows. *Quart. J. Roy. Meteor. Soc.*, **92,** 325–334.

Brugge, R., H. L. Jones, and J. C. Marshall, 1991: Non-hydrostatic ocean modelling for studies of open-ocean deep convection. *Proc. Workshop on Deep Convection and Deep Water Formation in the Oceans,* Elsevier Science, 325–340.

Chandresekhar, S., 1961: *Hydrodynamic Stability,* Dover.

Davey, M., and J. Whitehead, 1981: Rotating Rayleigh–Taylor instability as a model of sinking events in the ocean. *Geophys. Astrophys. Fluid Dyn.*, **17,** 237–253.

Dewar, W. K., 1987: Ventilating warm rings: Theory and energetics. *J. Phys. Oceanogr.*, **17,** 2219–2231.

——, and P. Killworth, 1991: On the cylindrical collapse problem, mixing and the merger of isolated eddies. *J. Phys. Oceanogr.*, **21,** 1563–1575.

Fernando, H. J. S., R.-R. Chen, and D. L. Boyer, 1991: Effects of rotation on convective turbulence. *J. Fluid. Mech.*, **228,** 513–547.

Gascard, J.-C., 1978: Mediterranean deep water formation, baroclinic instability and oceanic eddies. *Oceanol. Acta,* **1,** 315–330.

Haynes, P. H., and M. E. McIntyre, 1987: On the evolution of vorticity and potential vorticity in the presence of diabatic heating and frictional or other forces. *J. Atmos. Sci.*, **44,** 828–841.

Helfrich, C., and U. Send, 1988: Finite-amplitude evolution of two-layer geostrophic vortices. *J. Fluid Mech.*, **197,** 331–348.

——, and T. M. Battisti, 1991: Experiments on baroclinic vortex shedding from hydrothermal plumes. *J. Geophys. Res.*, **96**(C7), 12 511–12 518.

Hogg, N. G., and H. M. Stommel, 1985a: The heton, an elementary interaction between discrete baroclinic vortices, and its implication concerning eddy heat-flow. *Proc. Roy. Soc. London,* **A397,** 1–20.

——, and ——, 1985b: Hetonic explosions: The breakup and spread of warm pools as explained by baroclinic point vortices. *J. Atmos. Sci.*, **42,** 1465–1476.

Jones, H., and J. Marshall, 1993: Convection with rotation in a neutral ocean: A study of open-ocean deep convection. *J. Phys. Oceanogr.*, **23,**

Killworth, P. D., 1976: The mixing and spreading phases of MEDOC 1. *Progress in Oceanography,* Vol. 7, Pergamon, 59–90.

Marshall, J. C., and A. J. G. Nurser, 1992: Fluid dynamics of thermocline ventilation. *J. Phys. Oceanogr.*, **22,** 583–595.

Pedlosky, J., 1985: The instability of continuous heton clouds. *J. Atmos. Sci.*, **42,** 1477–1486.

Schott, F., and K. D. Leaman, 1991: Observations with moored acoustic Doppler current profilers in the convection regime in the Golfe du Lion. *J. Phys. Oceanogr.*, **21,** 558–574.

Stommel, H., A. D. Voorhis, and D. Webb, 1971: Submarine clouds in the deep ocean. *Am. Sci.*, **59,** 716–723.